

Large- p_T Photoproduction of $D^{*\pm}$ Mesons in ep Collisions

B.A. Kniehl¹, G. Kramer² and M. Spira³

¹ Max-Planck-Institut für Physik (Werner-Heisenberg-Institut),
Föhringer Ring 6, 80805 Munich, Germany

² II. Institut für Theoretische Physik*, Universität Hamburg,
Luruper Chaussee 149, 22761 Hamburg, Germany

³ Theoretical Physics Division, CERN,
1211 Geneva 23, Switzerland

Abstract

The cross section for the inclusive photoproduction of large- p_T $D^{*\pm}$ mesons is calculated at next-to-leading order, adopting different approaches to describe the fragmentation of charm quarks into $D^{*\pm}$ mesons. We treat the charm quark according to the massless factorization scheme, where it is assumed to be one of the active flavours inside the proton and the photon. We present inclusive single-particle distributions in transverse momentum and rapidity, including the contributions due to both direct and resolved photons. We compare and assess the various implementations of fragmentation. We argue that, in the high- p_T regime, a particularly realistic description can be obtained by convoluting the Altarelli-Parisi-evolved fragmentation functions of Peterson et al. with the hard-scattering cross sections of massless partons where the factorization of the collinear singularities associated with final-state charm quarks is converted to the massive-charm scheme. The predictions thus obtained agree well with recent experimental data by the H1 and ZEUS Collaborations at DESY HERA.

PACS numbers: 13.60.-r, 13.85.Ni, 13.87.Fh, 14.40.Lb

*Supported by Bundesministerium für Forschung und Technologie, Bonn, Germany, under Contract 05 7 HH 92P (5), and by EU Program *Human Capital and Mobility* through Network *Physics at High Energy Colliders* under Contract CHRX-CT93-0357 (DG12 COMA).

1 Introduction

Heavy-quark production in the ep colliding-beam experiments with DESY HERA offers a novel way of testing perturbative quantum chromodynamics (QCD). First results for the charm-quark photoproduction cross section $\sigma(\gamma p \rightarrow c\bar{c} + X)$ were presented by ZEUS [1] and H1 [2], and compared with a next-to-leading-order (NLO) calculation [3]. In this calculation, the massive-charm scheme has been adopted, in which the charm-quark mass $m \gg \Lambda_{QCD}$ acts as a cutoff and sets the scale for the perturbative calculation. The cross section factorizes into a partonic hard-scattering cross section multiplied by light-quark and gluon densities [4]. In this factorization approach, the only quarks inside the proton and the photon are the light ones. Thus, in the massive-charm scheme, the number of active flavours in the initial state is $n_f = 3$, while the massive charm quark appears only in the final state. For the prediction of the total charm photoproduction cross section, for which experimental results from HERA were presented in [1,2], this is the only possibility. Actually, $m \approx 1.5$ GeV is not very large compared to Λ_{QCD} , so that the validity of this approach is not obvious.

With the advent of new measurements, by H1 [2] and ZEUS [5], of the differential cross section $d^2\sigma/dy dp_T$ of inclusive $D^{*\pm}$ production, where y and p_T are the rapidity and transverse momentum of the $D^{*\pm}$ mesons, respectively, we have the possibility to test the theory in a different regime of scales. The experimental differential cross sections extend up to $p_T = 12$ GeV, so that, in contrast to the total-cross-section calculations, p_T rather than m should be considered as the large scale. Then, in NLO, terms proportional to $\alpha_s \ln(p_T^2/m^2)$ arise from collinear gluon emission by charm quarks or from almost collinear branching of gluons or photons into charm-anticharm pairs. For large enough p_T , these terms are bound to spoil the convergence of the perturbative series and cause large scale dependences of the NLO result at $p_T \gg m$. The proper procedure in the regime $p_T \gg m$ is to absorb the terms proportional to $\alpha_s \ln(p_T^2/m^2)$ into the charm distribution functions of the incoming photon and proton and into the fragmentation functions (FF's) of charm quarks into charmed hadrons. Of course, to perform this absorption, one needs information on the charm contribution in the parton density functions (PDF's) and FF's.

An alternative way of making reliable predictions at large p_T is to treat the charm quarks as massless partons. The collinear singularities corresponding to the $\alpha_s \ln(p_T^2/m^2)$ terms of the massive-charm scheme are then absorbed into the charm-quark PDF's and FF's in the same way as for the lighter u , d and s quarks. This massless approach was proposed in [6] and first applied to the production of large- p_T hadrons containing bottom quarks in $p\bar{p}$ collisions by Lampe [7] and by Cacciari and Greco [8]. Subsequently, it was employed in two independent studies of charm-quark photoproduction [9,10]. In these two investigations, the y and p_T distributions in the massless and massive approaches were compared with each other, making different assumptions concerning the initial state as well as the FF's in the massless approach. In [9], low- Q^2 electroproduction was considered, while [10] was concerned with photoproduction with fixed photon energy. In [9], the FF of the charm quark into charmed hadrons was approximated by $\delta(1-z)$, where $z = p_D/p_c$ is the scaled momentum of the charmed hadron D , whereas the authors of [10] employed

the perturbative FF's (PFF's) of [11], which they evolved from the starting scale m to the appropriate higher scales of order p_T according to the usual Altarelli-Parisi evolution equations.

It is the purpose of this work to remove the restriction to a scale-independent δ -type FF of the charm quark made in our previous study with Krämer [9] and to adopt more realistic descriptions of charm-quark fragmentation, including evolution to higher scales. Having extensively compared the massless and massive approaches in [9], we shall now focus our attention on the massless approach, which is likely to be more reliable in the large- p_T range, in which we are primarily interested here. Specifically, we shall consider the following models of charm-quark fragmentation: (i) δ -function-type FF without evolution [9] for reference; (ii) PFF [11] with and without evolution; and (iii) Peterson fragmentation [12] with evolution. Choice (iii) will be considered as the most realistic one and will be used for comparisons with the recent H1 [2] and ZEUS [5] data.

The outline of our work is as follows. In Section 2, we shall shortly describe the basic formalism of charm-quark fragmentation, discuss the transition from massless to massive factorization of final-state collinear singularities, and specify our assumptions concerning choices (i), (ii) and (iii). In Section 3, we shall investigate numerically the differences between the various implementations of charm-quark fragmentation discussed in Section 2. There, we also confront our final predictions based on the Peterson FF with the H1 and ZEUS data. Our conclusions will be summarized in Section 4.

2 Fragmentation function approach

In this section, we describe the underlying assumptions for the massless approach, making various choices for the FF's of the (anti)charm quark into $D^{*\pm}$ mesons. As is well known, two mechanisms contribute to the photoproduction of charm quarks in ep collisions: (i) In the direct photoproduction mechanism, the photon couples directly to the quarks, which, besides the massless u , d and s quarks, also include the massless c quark. In this case, no spectator particles travel along the momentum direction of the photon. (ii) In the resolved photoproduction mechanism, the photon splits up into a flux of u , d , s , c quarks and gluons, which then interact with the partons coming from the proton leading to the production of charm quarks at large p_T . The contributing parton-level processes are the same as in the case of charm-quark production in hadron-hadron collisions. The charm quark is accompanied by a spectator jet in the photon direction. Therefore, the γp cross section depends not only on the PDF's of the proton but also on those of the photon. The main difference relative to the usually considered massive-charm scheme is that the charm quark also contributes via the PDF's of the proton and photon, i.e. charm is already an active flavour in the initial state. In other words, there is no essential difference between the treatment of the truly light quarks u , d , s and the charm quark in the initial state. This approach is justified if a large scale is governing the production process. In our case, this is the p_T of the $D^{*\pm}$ mesons, with $p_T \gg m$. In this region, non-singular mass terms are suppressed in the cross sections by powers of m/p_T . The important mass terms appear

if the virtuality of the charm quark is small. This happens in the initial state if the charm quark is emitted from the proton or photon, and in the final state if the partons emit a $c\bar{c}$ pair. These two contributions lead to the $\alpha_s \ln(p_T^2/m^2)$ terms in the massive scheme. In our massless approach, they are summed into the scale-dependent PDF's and FF's of charm quarks into $D^{*\pm}$ mesons.

Thus, when we proceed to NLO, the following steps are taken: (i) The hard-scattering cross section for the direct- and resolved-photon processes are calculated in the massless approximation with $n_f = 4$ active flavours. The collinear singularities are subtracted according to the $\overline{\text{MS}}$ scheme. Since the charm quark is taken to be massless, the singularities from its splittings are subtracted as well.

(ii) The charm quark is accommodated in the PDF's of the proton and photon as a light flavour. The finite mass of the charm quark is taken into account by including it in the evolution in such a way that its PDF's are only non-vanishing above a scale set by its mass.

(iii) The FF's characterize the hadronization of the massless partons, including the charm quark, into mesonic or baryonic states containing the charm quark. In our case, these are the $D^{*\pm}$ mesons. Similarly to the fragmentation into light mesons, these FF's are basically non-perturbative input and must be determined by experiment, for example from the cross section of inclusive $D^{*\pm}$ production in e^+e^- annihilation [13]. This information determines the FF's at some starting scale, μ_0 .

An alternative that exploits the fact that the charm mass satisfies $m \gg \Lambda_{QCD}$ is the calculation of universal starting conditions for the FF's within perturbative QCD at a scale μ_0 of order m . The FF's thus obtained are the PFF's mentioned above. In [11], these starting conditions were calculated at NLO in the $\overline{\text{MS}}$ scheme. They read

$$\begin{aligned}
D_c^D(x, \mu_0) &= D_{\bar{c}}^{\bar{D}}(x, \mu_0) = \delta(1-x) + \frac{\alpha_s(\mu_0)}{2\pi} C_F \left\{ \frac{1+x^2}{1-x} \left[\ln \frac{\mu_0^2}{m^2} - 2 \ln(1-x) - 1 \right] \right\}_+, \\
D_g^D(x, \mu_0) &= D_g^{\bar{D}}(x, \mu_0) = \frac{\alpha_s(\mu_0)}{2\pi} T_f [x^2 + (1-x)^2] \ln \frac{\mu_0^2}{m^2}, \\
D_{q,\bar{q},c}^D(x, \mu_0) &= D_{q,\bar{q},c}^{\bar{D}}(x, \mu_0) = 0.
\end{aligned} \tag{1}$$

Here, D_i^D ($D_i^{\bar{D}}$) refers to the fragmentation of parton i into a hadron D (\bar{D}) containing a c (\bar{c}) quark, $C_F = 4/3$, $T_f = 1/2$, and $q = u, d, s$. The normalization of these FF's is such that D stands for the sum of all hadrons with a c quark. To obtain the FF into a specific charmed meson, for example the D^{*+} , we must include the branching ratio $B(c \rightarrow D^{*+})$.

(iv) For the higher scales $\mu > \mu_0$, the PDF's, the non-perturbative FF's and the PFF's are evolved in NLO up to the chosen factorization scale (which we take to be of order p_T) via the Altarelli-Parisi equations and convoluted with the NLO hard-scattering cross sections. The charm-quark mass m then only enters in terms of the starting conditions of the PDF's and FF's.

As already mentioned, the large logarithmic terms proportional to $\ln(p_T^2/m^2)$, which appear in the massive scheme, are resummed in this approach. To be specific, they are effectively split into two parts. One part proportional to $\ln(p_T^2/\mu^2)$, where μ is some generic

factorization scale, appears in the hard-scattering cross sections having no dependence on m . This part may be kept small by choosing $\mu \approx p_T$. The other part, proportional to $\ln(\mu^2/m^2)$, is absorbed into the PDF's and FF's. The logarithm $\ln(\mu^2/\mu_0^2)$, which is large if $\mu_0 \approx m$ and $\mu \approx p_T$, is incorporated via the evolution equations and therefore resummed. The residual term proportional to $\ln(\mu_0^2/m^2)$, connected with the starting conditions in (1), is treated with fixed-order perturbation theory in the case of the PFF's, or is part of the non-perturbative input in the case of general FF's.

The PFF's given in terms of the starting conditions (1) suggest some simplifications which we consider as reasonable approximations for the PFF's. The dominant term in (1) is the δ function expressing the fact that, due to $m \gg \Lambda_{QCD}$, the charm quark transforms into the charmed hadron having the same momentum, any binding effect of the light quark of order Λ_{QCD} being neglected. The approximation $D_c^D(x, \mu) = \delta(1-x)$, denoted A for later use, was considered in our earlier work [9]. This approximation neglects the important $\ln(\mu^2/\mu_0^2)$ terms induced in the FF's through the evolution. Unless otherwise stated, we shall choose $\mu_0 = 2m$ and $\mu = 2m_T$, where $m_T = \sqrt{m^2 + p_T^2}$ is the transverse mass of the produced hadron.

Approximation B consists of keeping all terms in (1), but with the replacement $\mu_0 = \mu$. This approximation includes the large $\ln(\mu^2/m^2)$ terms to fixed order in α_s , i.e. not in the resummed form because the FF's are not evolved up to the scale μ via the evolution equations. Except for the fact that the proton and photon PDF's still have four active flavours, this approximation is, from the conceptual point of view, most closely related to the massive scheme [3,9], in the sense that the important mass terms of the massive calculation, namely the logarithmic ones related to the collinear would-be singularities, are properly included, while the non-singular power terms in m/p_T are omitted. We stress that the latter are indispensable if p_T is of order m , and must be included if total cross sections are to be calculated; approximation B is then bound to break down. However, our goal is to improve the theoretical description at $p_T \gg m$. Since, in case B , the FF's are not evolved to higher scales according to the evolution equations, the terms proportional to α_s in (1) may be shifted to the hard-scattering cross section, which we actually choose to do. In fact, case B may be viewed as a change of factorization scheme, in the sense that the factorization of the final-state collinear singularities associated with the charm quark is adjusted so as to match the finite- m calculation. This is an equivalent interpretation of the matching procedure proposed in [11] between the massless-charm calculation in connection with the PFF's and the massive-charm calculation without FF's. Specifically, we substitute in the hard-scattering cross sections $\alpha_s(\mu)P_{ci}^{(0,T)}(x) \ln(s/\mu^2) \rightarrow \alpha_s(\mu)P_{ci}^{(0,T)}(x) \ln(s/\mu^2) - \alpha_s(\mu_0)d_{ci}(x)$, where $P_{ci}^{(0,T)}(x)$ are the timelike LO $i \rightarrow c$ splitting functions [14] and $d_{ci}(x)$ may be gleaned from (1):

$$\begin{aligned} d_{cc}(x) &= -C_F \left\{ \frac{1+x^2}{1-x} \left[\ln \frac{\mu_0^2}{m^2} - 2 \ln(1-x) - 1 \right] \right\}_+ \\ &= -P_{qq}^{(0,T)}(x) \ln \frac{\mu_0^2}{m^2} + C_F \left\{ -2\delta(1-x) + 2 \left(\frac{1}{1-x} \right)_+ + 4 \left[\frac{\ln(1-x)}{1-x} \right]_+ \right\} \end{aligned}$$

$$\begin{aligned}
& - (1+x) [1 + 2 \ln(1-x)] \Big\}, \\
d_{cg}(x) &= -T_f [x^2 + (1-x)^2] \ln \frac{\mu_0^2}{m^2} \\
&= -P_{qg}^{(0,T)}(x) \ln \frac{\mu_0^2}{m^2}, \\
d_{cq}(x) &= d_{c\bar{q}}(x) = d_{c\bar{c}}(x) = 0,
\end{aligned} \tag{2}$$

with $q = u, d, s$. The $d_{\bar{c}i}$ functions emerge by charge conjugation. Since the PFF's of (1) refer to the $\overline{\text{MS}}$ factorization scheme for the collinear singularities associated with outgoing massless-charm lines, so do the d_{ij} functions of (2). In case B , $\ln(\mu_0^2/m^2) \approx \ln(p_T^2/m^2)$ is large. Leaving aside the terms in (2) that are not enhanced by this logarithm, case B obviously amounts to choosing the final-state factorization scale in the massless-charm hard-scattering cross sections to be $\mu = m$ and omitting the d_{ij} functions, i.e. to choosing the final-state factorization scale in case A to be $\mu = m$. In our implementation of case B , we have $D_c^D(x, \mu) = \delta(1-x)$ for all factorization scales μ , just as in case A .

Obviously, case B may be refined by resumming the large logarithms $\ln(p_T^2/m^2)$ via evolution. To this end, in case C , we take $D_c^D(x, \mu_0) = \delta(1-x)$ as the input distribution at the starting scale μ_0 for the NLO evolution up to μ . At the same time, we keep the d_{ij} functions, with the large logarithm stripped off, i.e. with μ_0 now of order m rather than p_T , in the hard-scattering cross sections.

An alternative refinement of case B may be obtained by taking the full PFF distributions of (1) as input for the evolution up to scale μ , and convoluting the outcome with the massless-charm hard-scattering cross sections (without d_{ij} functions). This approach, which we denote by D , corresponds to the PFF approach advocated in [11] for inclusive heavy-quark production via e^+e^- annihilation. It was applied to inclusive bottom-quark production in $p\bar{p}$ collisions in [8] and to inclusive charm-quark production in γp and $\gamma\gamma$ collisions in [10,15], respectively.

However, it is not at all clear that the PFF's give the correct description for the fragmentation of the charm quark into charmed hadrons, since the charm quark is only moderately heavy. Although the average value $\langle x \rangle$ near $\mu = \mu_0$ is not precisely known, it is bound to be $\langle x \rangle < 1$. Most measurements of $\langle x \rangle$ are at larger scales. In the case of $c \rightarrow D^{*+}$, we have $\langle x \rangle = 0.495_{-0.011}^{+0.010}(\text{stat.}) \pm 0.007(\text{sys.})$ from ALEPH [16] and $\langle x \rangle = 0.515_{-0.005}^{+0.008}(\text{stat.}) \pm 0.010(\text{sys.})$ from OPAL [17] at $\mu = 91.2$ GeV, and $\langle x \rangle = 0.73 \pm 0.05$ at $\mu = 10$ GeV [18], indicating that $\langle x \rangle < 1$ at $\mu = \mu_0$ as well. Therefore, the distribution by Peterson et al. [12] is usually considered to be a better approximation for the FF at the starting scale μ_0 . It has the form

$$D_c^D(x, \mu_0) = \mathcal{N} \frac{x(1-x)^2}{[(1-x)^2 + \epsilon x]^2}. \tag{3}$$

Apart from the normalization \mathcal{N} , it depends just on the parameter ϵ , which is related to $\langle x \rangle$. Note that (3) turns into a δ function in the limit $\epsilon \rightarrow 0$. We choose $\epsilon = 0.06$, which

is the central value obtained in [19] for charm quarks. In case E , we adopt (3) with

$$\mathcal{N}^{-1} = \frac{(\epsilon^2 - 6\epsilon + 4)}{(4 - \epsilon)\sqrt{4\epsilon - \epsilon^2}} \left\{ \arctan \frac{\epsilon}{\sqrt{4\epsilon - \epsilon^2}} + \arctan \frac{2 - \epsilon}{\sqrt{4\epsilon - \epsilon^2}} \right\} + \frac{1}{2} \ln \epsilon + \frac{1}{4 - \epsilon}, \quad (4)$$

so that $\int_0^1 dx D_c^D(x, \mu_0) = 1$. For $\epsilon = 0.06$, one has $\mathcal{N} \approx 0.625$. This simplifies the comparison with the fragmentation models A – D . In Section 3.4, where we compare our predictions with the HERA data, we must adjust the normalization of our calculation by including the measured branching fraction $B(c \rightarrow D^{*+})$ [17].

The Peterson FF for $c \rightarrow D^{*+}$ fragmentation of (3) has also been used in [20] for calculating the production of $D^{*\pm}$ mesons in γp collisions based on the purely massive scheme. In our approach, we need the evolved FF's at the scale μ , with (3) describing the input at the starting scale μ_0 . We solve the evolution equations using moments in Mellin space. For the reader's convenience, the moments of (3) are listed in Appendix A. They are expressed in terms of hypergeometric functions of complex arguments, which are conveniently calculated from appropriate series expansions, also written down in Appendix A. To account for the fact that the Peterson FF describes the transition from a massive charm quark into a physical D^{*+} meson, whereas, for reasons explained in the Introduction, we work with hard-scattering cross sections where the charm quark is treated as a massless flavour, we incorporate the d_{ij} functions of (2) in our analysis just as we do in case C . This means that case E emerges from case C by replacing the δ -function-type input distribution at scale μ_0 with the Peterson formula of (3).

An alternative approach would be to include the terms relating the massless and massive schemes in the evolution of the FF as we do in version D , where we evolve the full PFF's of (1). In other words, one would convolute the PFF's with the Peterson formula (3) at the scale μ_0 , evolve these modified initial distributions at NLO up to the scale μ and employ the FF's thus obtained in the usual massless-charm $\overline{\text{MS}}$ analysis (without d_{ij} functions). In the following, this possible alternative for scheme E will be called scheme F . Both of these schemes properly resum the large logarithmic terms of the type $\ln(\mu^2/\mu_0^2)$ which emerge from (1) as μ_0 is driven up to μ . In scheme E , just the latter logarithms get resummed, while the non-logarithmic terms of (1) are treated in fixed-order perturbation theory. By contrast, in scheme F , also these non-logarithmic terms are included in the evolution. Scheme E is minimal in the sense that it allows us to include in the evolution just the long-distance part of the $c \rightarrow D^{*+}$ fragmentation process, which is encoded in the Peterson ansatz (3). We shall adopt scheme E whenever we confront theoretical predictions with HERA data. In the limit $\epsilon \rightarrow 0$, cases E and F coincide with cases C and D , respectively. For a given value of ϵ , one expects the difference between schemes E and F to be similar to the one between schemes C and D . Since schemes C and D do not yield physical observables, their difference is phenomenologically inconsequential. By the same token, it is unreasonable to expect that a cross section evaluated in schemes C or D should coincide with the corresponding charm-quark production cross section obtained in the all-massive scheme. In the case of $D^{*\pm}$ photoproduction, this is even more apparent, since the cross sections of schemes C and D exhibit a significant sensitivity to the charm content of the resolved photon (intrinsic charm), which does not enter the all-massive

calculation at all. On the other hand, the difference between schemes E and F is to be compensated by a corresponding shift in the ϵ parameter of (3), i.e. ϵ is scheme dependent at NLO. For instance, if one wishes to use the value of ϵ determined through a NLO fit to e^+e^- data as input for a NLO prediction of photoproduction, one has to make sure that both analyses are carried out in the same scheme. Only then, one may obtain a coherent description of high-energy e^+e^- data and high- p_T ep data. We emphasize that, on the basis of an all-massive calculation including fragmentation, this cannot be achieved in any meaningful way, due to the presence of sizeable logarithms at fixed order. A consistent procedure within the all-massive framework would be to determine ϵ from a NLO fit to low-energy e^+e^- data on inclusive $D^{*\pm}$ production, which has not been done so far.

A second alternative to case E has been adopted in [21] to describe charmed-meson production at the Tevatron. In [21], the evolved PFF's are convoluted with some unevolved x distribution of the form $N(1-x)^\alpha x^\beta$. By contrast, we assume that the non-perturbative x distribution of the D^{*+} mesons, where x is the longitudinal-momentum fraction w.r.t. the quasi-massive parent charm quarks, is subject to evolution.

The calculation of the hard-scattering cross sections proceeds along the lines of our previous works [9,22] on the basis of the direct- and resolved-photon hard-scattering cross section obtained in [23] and [24], respectively.

3 Results

This section consists of four parts. First, we specify our assumptions concerning the proton and photon PDF's as well as the equivalent photon approximation. Second, we describe the various degrees of refinement in the treatment of fragmentation. Third, we discuss various theoretical uncertainties related to the proton and photon PDF's and the dependence on scales and parameters intrinsic to the FF's. Finally, in the fourth part, we present our predictions for the inclusive $D^{*\pm}$ photoproduction under realistic kinematic conditions corresponding to the H1 and ZEUS experiments.

3.1 Input information

For the calculation of the cross section $d^2\sigma/dy_{lab} dp_T$, we adopt the present standard HERA conditions, where $E_p = 820$ GeV protons collide with $E_e = 27.5$ GeV positrons in the laboratory frame. We sum over D^{*+} and D^{*-} mesons. We take y_{lab} , which refers to the laboratory frame, to be positive in the proton flight direction. The quasi-real-photon spectrum is described in the Weizsäcker-Williams approximation with the formula

$$f_{\gamma/e}(x) = \frac{\alpha}{2\pi} \left[\frac{1 + (1-x)^2}{x} \ln \frac{Q_{max}^2}{Q_{min}^2} + 2m_e^2 x \left(\frac{1}{Q_{max}^2} - \frac{1}{Q_{min}^2} \right) \right], \quad (5)$$

where $x = E_\gamma/E_e$, $Q_{min}^2 = m_e^2 x^2/(1-x)$, α is Sommerfeld's fine-structure constant and m_e is the electron mass. In the case of ZEUS, where the final-state positron is not detected (ZEUS untagged), one has $Q_{max}^2 = 4 \text{ GeV}^2$ and $0.147 < x < 0.869$, which corresponds

to γp centre-of-mass (CM) energies of $115 \text{ GeV} < W < 280 \text{ GeV}$ [5]. We shall use these conditions for the evaluation of the cross sections in the next two subsections. Besides the untagged case, the H1 Collaboration has also presented data where the positron is tagged. The corresponding parameters will be specified later. Our default sets for the proton and photon PDF's are CTEQ4M [25], with $\Lambda_{\overline{\text{MS}}}^{(4)} = 296 \text{ MeV}$, and GRV [26]. We work at NLO in the $\overline{\text{MS}}$ scheme with $n_f = 4$ flavours. We identify the factorization scales associated with the proton, photon and final-state hadron, M_p , M_γ and M_h , respectively, and collectively denote them by M_f . Our standard choice of renormalization and factorization scales is $\mu = \xi m_T$ and $M_f = 2\xi m_T$ with $\xi = 1$. If the FF's are evolved, we take the starting scale to be $\mu_0 = 2m$ with $m = 1.5 \text{ GeV}$. We calculate $\alpha_s(\mu)$ from the two-loop formula with $\Lambda_{\overline{\text{MS}}}^{(4)}$ equal to the value used in the proton PDF's.

3.2 Refinements in fragmentation

In our previous work [9], we made the most simple ansatz for the fragmentation of charm quarks into charmed hadrons, namely $D_c^D(x, \mu) = \delta(1-x)$ for all scales μ . In Section 2, this was referred to as case *A*. In Figs. 1 and 2, we show the predictions for $d\sigma/dp_T$ integrated over $-1.5 < y_{lab} < 1$ and $d^2\sigma/dy_{lab} dp_T$ at $p_T = 7 \text{ GeV}$, respectively, according to this case together with the refinements *B–F* discussed in the same section, adopting the ZEUS untagged conditions. Cases *B* and *C* differ from case *A* in that they take the evolution into account. In the rough approximation of case *B*, the evolution is incorporated by choosing $\mu_0 = M_h$ in the definitions (2) of the d_{ij} functions, which correct for massive final-state factorization in the hard-scattering cross sections. This generates large logarithms of the form $\ln(M_h^2/m^2)$, which are resummed in case *C* by properly evolving the δ -type FF's from the starting scale $\mu_0 = 2m$ up to M_h . In case *C*, the transition to the massive factorization is performed by adding the d_{ij} functions with $\mu_0 = 2m$. In contrast to the case *B*, case *C* includes also contributions from gluon fragmentation and, to a lesser extent, from light-quark fragmentation. In case *D*, the hard-scattering cross sections in the massless factorization scheme ($d_{ij} = 0$) are convoluted with the evolved PFF's of (1). The effect of the d_{ij} functions is then contained in the PFF's.

We see in Fig. 1 that, at low p_T , the latter three cases (*B*, *C* and *D*) give very similar cross sections $d\sigma/dp_T$, whereas there are appreciable differences at large p_T , especially between cases *C* and *D*. Case *D* exhibits the strongest fall-off. Here not only the δ function, but also the finite, perturbative terms of (1) are included in the evolution. Case *B*, where evolution is accounted for only in the leading-logarithmic approximation, has the smallest decrease of $d\sigma/dp_T$ with increasing p_T . Case *C*, where only the δ function is evolved, lies between cases *B* and *D*, as one would expect, but closer to case *B*. We emphasize that the evolution of the FF's is performed up to NLO (cases *C* and *D*). We conclude from this study that the evolution of the FF must be fully taken into account in order to obtain realistic predictions for the p_T distribution. The unevolved δ -function fragmentation considered in [9] (case *A*) is unreliable for large p_T .

In [9], case *A* was compared with the massive NLO calculation, adopting the previous ZEUS conditions, which are very similar to the present ones used here. The massive NLO

result turned out to be roughly 45% of the case-*A* result. On the other hand, from Fig. 1 we see that, at $p_T = 3$ GeV (12 GeV), the case-*B* result amounts to 67% (54%) of the case-*A* result. In other words, at $p_T = 3$ GeV (12 GeV), the massive NLO result is roughly $2/3$ ($5/6$) of the case-*B* result. This may be partly attributed to the negative contribution from the power terms in m/p_T , which are not included in case *B*. The magnitude of these terms rapidly decreases with increasing p_T . On the other hand, in contrast to the massive calculation, case *B* receives contributions from the charm quarks intrinsic to the proton and photon. These contributions will be investigated in Figs. 4 and 5, respectively. We shall see that the charm content of the photon is particularly important.

The rapidity distributions at $p_T = 7$ GeV for the cases *A*, *B*, *C* and *D* are shown in Fig. 2. Here the pattern is somewhat different. In the y_{lab} region where the cross section $d^2\sigma/dy_{lab} dp_T$ is maximal, i.e. $-1.5 < y_{lab} < 1$, the distributions of cases *A*, *B*, *C* and *D* have very similar shapes. The overall normalizations just differ according to the hierarchy in Fig. 1. For the larger rapidities $y_{lab} > 2$, the cross sections for cases *A*, *B*, *C* and *D* almost coincide, i.e. here the evolution of the FF's has little effect.

In Figs. 1 and 2, we have also included the predictions based on the Peterson FF evolved to larger scales in NLO, corresponding to cases *E* and *F*. This FF is also normalized to unity, as all the other FF's, in order to facilitate the comparison. That is, in the limit $\epsilon \rightarrow 0$, the results of cases *E* and *F* coincide with those of cases *C* and *D*, respectively. As anticipated in Section 2, for finite ϵ , the relative difference between cases *E* and *F* is very similar to that between cases *C* and *D*. In particular, the p_T distributions for cases *E* and *F* in Fig. 1 converge towards the low- p_T end, where the non-logarithmic terms of the PFF's as implemented in case *F* are just mildly affected by the evolution. The main effect of the Peterson FF with finite ϵ is to reduce the overall normalization of the respective calculations.

In the following investigations, we shall stick to case *E* and employ the NLO-evolved Peterson FF. This description of charm fragmentation is more realistic than the PFF's because the charm quark is only moderately heavy. Compared with the massive-charm scheme, the massless-charm scheme shows a completely different decomposition of the cross section into direct- and resolved-photon contributions. This was analysed in detail in our earlier work [9]. Whereas in the massive approach direct photoproduction is dominant at large p_T , in our massless scheme both contributions are of the same order of magnitude [9]. This is demonstrated in Fig. 3 for $d^2\sigma/dy_{lab} dp_T$ at $p_T = 7$ GeV. Both cross sections peak approximately at $y_{lab} = 0$. The resolved cross section has in addition a shoulder at larger y_{lab} , which originates from the gluon part of the photon PDF's. The peak at $y_{lab} = 0$ is due to the charm part, as may be inferred from Fig. 5. Of course, we must bear in mind that the decomposition of the photoproduction cross section in direct- and resolved-photon contributions is ambiguous at NLO; it depends on the factorization scheme and scale, which we take to be the $\overline{\text{MS}}$ scheme and $M_\gamma = 2m_T$, respectively. However, the sum of the two contributions is unambiguously defined.

3.3 Theoretical uncertainties

Before we compare our results with recent experimental data from H1 and ZEUS, we investigate several theoretical uncertainties, which might be relevant. First, we consider the influence of the proton PDF's. In Fig. 4, the cross section $d^2\sigma/dy_{lab} dp_T$ at $p_T = 7$ GeV is plotted for our standard CTEQ4M [25] proton PDF's and compared with the result obtained using the recent proton PDF set MRS(G) by the Durham group [27], with $\Lambda_{\overline{\text{MS}}}^{(4)} = 254$ MeV. The cross sections for these two choices are almost identical. From this we conclude that our predictions are insignificantly influenced through our choice of the proton PDF's. In Fig. 4, we also show the influence of the charm distribution inside the proton. If it is taken away from the CTEQ4M PDF's, the cross section hardly changes. Only for larger y_{lab} , where the cross section is small, do we see the effect of the charm content of the proton.

A similar study w.r.t. the photon PDF's is presented in Fig. 5. Here we compare $d^2\sigma/dy_{lab} dp_T$ at $p_T = 7$ GeV, evaluated with our standard GRV photon PDF's, with the calculation based on the recently published new version of the photon PDF's by Gordon and Storrow [28]. The cross sections differ somewhat, by typically 10–20%, over the whole y_{lab} range. This means that very accurate data are needed if the differences between the GRV and GS photon PDF's are to be disentangled. In Fig. 5, we have also plotted the GRV prediction with the charm distribution inside the photon put to zero. This has a dramatic effect. For $y_{lab} < 1$, the curves for the direct-photon contribution and the sum of the direct and resolved contributions are almost identical. This shows that the resolved cross section is essentially made up by the charm content of the photon. Only for $y_{lab} > 1$, where the cross section decreases with increasing y_{lab} , can we see the effect of the other components of the photon, i.e. the gluon and the light quarks. Therefore charmed-hadron photoproduction at large p_T seems to be an ideal place to learn specifically about the charm content of the photon [9,29], which otherwise can only be studied in charmed-hadron production in large- Q^2 $e\gamma$ scattering.

All finite-order perturbative calculations are plagued by scale dependences. Although we may expect that this dependence is reduced in NLO, it is not in general negligible, in particular at moderate p_T . In Fig. 6, we show the cross section $d^2\sigma/dy_{lab} dp_T$ at $p_T = 7$ GeV for our standard PDF choice and scales $\mu = M_f/2 = \xi m_T$ with $\xi = 1/2, 1$ and 2. In all these cases, we keep the constraint $\mu_0 = 2m$. This scale variation produces changes of the cross section of only $\pm 10\%$, which indicates good perturbative stability. The maximum change occurs where the cross section is maximal. The main effect is actually due to the variation of the renormalization scale. In fact, if we stick to $\mu = m_T$, but choose $M_f = m_T$ instead of $M_f = 2m_T$, we observe only a small difference in the cross section; compare the dotted and full curves in Fig. 6.

The cross section for the production of charmed hadrons depends on the choice of FF's. This was already demonstrated in Figs. 1 and 2, where we compared the cross sections for different assumptions concerning the FF's. Possibly, the choice $\epsilon = 0.06$ in the Peterson FF, which we have adopted from [19], might not be fully compatible with our procedure. In particular, the value of ϵ must depend on the value of the initial scale

μ_0 . Up to now, we have fixed $\mu_0 = 2m$ and $\epsilon = 0.06$. In Fig. 7, we study how variations in μ_0 and ϵ affect the cross section $d^2\sigma/dy_{lab} dp_T$ at $p_T = 7$ GeV. If we reduce μ_0 to $\mu_0 = m$ keeping $\epsilon = 0.06$, the cross section decreases, as may be seen by comparing the dotted curve with the full one. This reduction can be compensated by simultaneously adjusting ϵ to a smaller value. The variation of the cross section with ϵ may also be inferred from Fig. 7, where $\epsilon = 0.04, 0.06$ and 0.08 are considered. Decreasing ϵ leads to a larger cross section. This may be understood by observing that case C emerges from case E in the limit $\epsilon \rightarrow 0$. In order to obtain definite predictions, we must use the information on the ϵ parameter in connection with a fixed choice for μ_0 from other $D^{*\pm}$ production experiments, e.g. from $e^+e^- \rightarrow D^{*\pm} + X$. So far, the choice $\epsilon = 0.06$ was motivated by Chrin's analysis [19] of charmed-meson production in the PETRA energy range. This analysis relied on fragmentation models. Therefore it is unclear whether $\epsilon = 0.06$ is the correct choice for the Peterson FF at $\mu_0 = 2m$. We shall come back to this point when we compare our calculation with the experimental data from H1 and ZEUS.

3.4 Comparison with H1 and ZEUS data

In this section, we compare our NLO predictions for the cross section of inclusive $D^{*\pm}$ photoproduction in ep scattering at HERA with three recent sets of data: a) H1 tagged, b) H1 untagged [2] and c) ZEUS untagged [5]. We sum over D^{*+} and D^{*-} mesons and adjust the normalization of the Peterson FF by including the measured branching fraction $B(c \rightarrow D^{*+}) = B(\bar{c} \rightarrow D^{*-}) = 0.260$ [17]. We adopt the respective experimental constraints on the equivalent photon spectrum of (5): a) $0.28 < x < 0.65$, $Q_{max}^2 = 0.01$ GeV², b) $0.1 < x < 0.8$, $Q_{max}^2 = 4$ GeV² [2] and c) $0.147 < x < 0.869$, $Q_{max}^2 = 4$ GeV² [5]. We first consider the p_T distribution $d\sigma/dp_T$ integrated over the rapidity interval $-1.5 < y_{lab} < 1$. In Figs. 8a–c, we confront the H1 tagged, H1 untagged and ZEUS untagged data with our respective NLO predictions. The renormalization and factorization scales are chosen to be $\mu = M_f/2 = \xi m_T$ with $\xi = 1/2$ (dashed lines), $\xi = 1$ (solid lines) and $\xi = 2$ (dash-dotted lines). We observe that the scale dependence is small, approximately $\pm 10\%$, indicating that corrections beyond NLO are likely to be negligible. In all three cases, the agreement with the data is remarkably good, even at small p_T , where we would not have expected it. In our approach, the p_T spectra come out somewhat larger than in the all-massive theory [20] which was used for comparison in [2,5] and therefore agree slightly better with the data. In the low- p_T range, this may be partly attributed to the omission of the power terms in m/p_T in our approach.

It is well known that the rapidity distribution $d^2\sigma/dy_{lab} dp_T$ at fixed p_T usually allows for a more stringent test of the theory than $d\sigma/dp_T$. Unfortunately, the measured y_{lab} distributions available so far all correspond to $d^2\sigma/dy_{lab} dp_T$ integrated over p_T intervals with rather small lower bounds, namely $2.5 \text{ GeV} < p_T < 10 \text{ GeV}$ in the case of H1 [2] and $3 \text{ GeV} < p_T < 12 \text{ GeV}$ in the case of ZEUS [5]. The corresponding H1 tagged, H1 untagged and ZEUS untagged data are compared with our NLO predictions for $\xi = 1/2, 1$ and 2 in Figs. 9a–c, respectively. The theoretical predictions for H1 tagged and H1 untagged are quite different. The curves for the tagged case have their maxima at smaller y_{lab} , close

to $y_{lab} = -1.2$, and exhibit a much stronger variation with y_{lab} than the curves for the untagged case, which reach their maxima near -0.5 . This difference may be understood by observing that the soft end of the equivalent photon spectrum is eliminated in the tagged case by the cut $x > 0.28$. The agreement between theory and data is worse than in the case of $d\sigma/dp_T$. On the other hand, the experimental errors are still rather large. We observe that in all three cases there is perfect agreement in the central region of the detector, at $y_{lab} = -0.25$, whereas in the backward direction the theoretical predictions tend to slightly overshoot data, especially in the case of H1. In the case of ZEUS, where the lower cut on p_T is somewhat larger than for H1, our prediction agrees slightly better with the data than the result of the all-massive calculation presented in Fig. 4 of [5]. However, this observation has to be taken with a grain of salt, since the bulk of the cross section is accumulated at the low- p_T end, where our approach is expected to be less reliable.

In the comparison of the data with our predictions, we have to keep in mind that the latter depend on the parameter ϵ and the starting scale μ_0 of the Peterson FF. We have chosen $\epsilon = 0.06$ and $\mu_0 = 2m$. In Fig. 7, we have seen that varying ϵ by ± 0.02 changes the cross section by $\pm 15\%$, which is comparable to the scale dependence. We have verified by explicit calculation that the choice $\epsilon = 0.06$ in conjunction with $\mu_0 = 2m$ yields a satisfactory global fit to the $\langle x \rangle$ values measured in e^+e^- experiments with CM energies between 10 and 91.2 GeV. We conclude that, at the present stage, the comparison between theory and data is not jeopardized by the uncertainty in ϵ .

4 Summary and Conclusions

In this work, we calculated the cross section of inclusive $D^{*\pm}$ -meson production via small- Q^2 ep scattering at HERA energies on the basis of a new massless-charm approach. Specifically, the $\overline{\text{MS}}$ factorization of the collinear singularities associated with massless charm quarks in the final state is adjusted so as to match the corresponding massive-charm calculation. This is implemented in a way similar to switching from the $\overline{\text{MS}}$ factorization scheme e.g. to the deep-inelastic-scattering (DIS) scheme within the massless analysis. The fragmentation of the quasi-massive charm quarks into the physical D^{*+} mesons at long distances is then described by the NLO-evolved Peterson FF with a suitable choice of ϵ at the starting scale μ_0 . Compared to the all-massive calculation, this has the advantage that the large logarithms $\ln(p_T^2/m^2)$ are resummed, in particular through the appearance of a much more sizeable resolved-photon contribution. We believe that this massless-charm scheme is much more suitable in the large- p_T regime. Furthermore, it offers us the opportunity to investigate the charm distribution inside the resolved photon (see Fig. 5), which does not enter the all-massive calculation.

We studied various refinements of the massless-charm approach w.r.t. the description of the $c \rightarrow D^{*+}$ fragmentation. The most realistic fragmentation model, based on the Peterson FF evolved through NLO evolution equations from the starting scale $\mu_0 = 2m$ up to the characteristic scale of the process, was examined in great detail and used for

comparisons with recent data from the H1 and ZEUS Collaborations at HERA. We found good agreement, in particular for the p_T spectra as well as the y_{lab} spectra in the central region. Surprisingly, even at rather low p_T , some of our predictions agree with the data slightly better than those obtained within the all-massive scheme (compare Figs. 8c and 9c with Fig. 4 of [5]), which may be an artifact of neglecting the non-singular power terms in m/p_T . Since our approach is better justified theoretically for $p_T \gg m$, we hope that HERA data on inclusive $D^{*\pm}$ photoproduction in the large- p_T region will soon be available with high statistics. In particular, y_{lab} spectra with large minimum- p_T cuts would allow for a more stringent test of our fragmentation model in particular and the QCD-improved parton model in general, and increase our understanding of the charm distribution inside the resolved photon.

If one determines ϵ from an NLO fit to e^+e^- data, the result will depend on whether scheme E or scheme F is adopted. According to the factorization theorem, this difference is expected to be compensated if one makes NLO predictions for different kinds of experiments as long as one works in the respective scheme. By the same token, NLO predictions based on the all-massive scheme with Peterson fragmentation [20] suffer from an essentially uncontrolled normalization as long as the ϵ parameter is not fitted within the same scheme.

After the completion of this work, new sets of $D^{*\pm}$ FF's have been extracted from fits to e^+e^- data adopting scheme E [30] and a variant of scheme F [31].

ACKNOWLEDGMENTS

One of us (GK) thanks the Theory Group of the Werner-Heisenberg-Institut for the hospitality extended to him during a visit when this paper was finalized. One of us (MS) thanks P. Nason for useful discussions about [11].

A Mellin transform of the Peterson fragmentation function

The Mellin transform of a distribution function, $D(x)$, is defined as

$$\tilde{D}(N) = \int_0^1 dx x^{N-1} D(x), \quad (6)$$

where N is complex. Taking $D(x)$ to be the Peterson FF of (3), we find

$$\begin{aligned} \tilde{D}(N) = \frac{2\mathcal{N}}{(N+1)(N+2)(N+3)} & \left[\frac{{}_2F_1(2, 3; N+4; x_1^{-1})}{x_1^2(x_1-x_2)^2} + \frac{{}_2F_1(2, 3; N+4; x_2^{-1})}{x_2^2(x_1-x_2)^2} \right. \\ & \left. + 2 \frac{{}_2F_1(1, 3; N+4; x_1^{-1})}{x_1(x_1-x_2)^3} - 2 \frac{{}_2F_1(1, 3; N+4; x_2^{-1})}{x_2(x_1-x_2)^3} \right], \quad (7) \end{aligned}$$

where \mathcal{N} is the normalization factor in (3),

$${}_2F_1(a, b; c; z) = \frac{\Gamma(c)}{\Gamma(b)\Gamma(c-b)} \int_0^1 dx x^{b-1} (1-x)^{c-b-1} (1-xz)^{-a} \quad (8)$$

is the hypergeometric function and

$$x_{1/2} = \frac{\epsilon}{2} \left(1 \pm i \sqrt{\frac{4}{\epsilon} - 1} \right). \quad (9)$$

The following expansion is useful for numerical purposes:

$$\begin{aligned} {}_2F_1(a, a+m; c; z) &= \frac{\Gamma(c)(-z)^{-a-m}}{\Gamma(a+m)\Gamma(c-a)} \sum_{n=0}^{\infty} \frac{(a)_{m+n}(1-c+a)_{m+n}}{n!(m+n)!} z^{-n} [\ln(-z) \\ &\quad + \psi(1+m+n) + \psi(1+n) - \psi(a+m+n) - \psi(c-a-m-n)] \\ &\quad + (-z)^{-a} \frac{\Gamma(c)}{\Gamma(a+m)} \sum_{n=0}^{m-1} \frac{\Gamma(m-n)(a)_n}{n!\Gamma(c-a-n)} z^{-n}, \end{aligned} \quad (10)$$

where

$$\psi(x) = \frac{\Gamma'(x)}{\Gamma(x)} \quad (11)$$

is the digamma function and

$$(a)_n = \frac{\Gamma(a+n)}{\Gamma(a)} \quad (12)$$

is Pochhammer's symbol.

References

- [1] M. Derrick et al. (ZEUS Collaboration): Phys. Lett. B 349 (1995) 225
- [2] S. Aid et al. (H1 Collaboration): Nucl. Phys. B 472 (1996) 32
- [3] S. Frixione, M.L. Mangano, P. Nason, G. Ridolfi: Nucl. Phys. B 412 (1994) 225; Phys. Lett. B 348 (1995) 633
- [4] J.C. Collins, D.E. Soper, G. Sterman: Nucl. Phys. B 263 (1986) 37
- [5] J. Breitweg et al. (ZEUS Collaboration): Contributed Paper No. pa05-051 to the 28th International Conference on High Energy Physics, Warsaw, Poland, 25-31 July 1996; Phys. Lett. B 401 (1997) 192; U. Karshon (private communication).
- [6] P. Nason, S. Dawson, R.K. Ellis: Nucl. Phys. B 327 (1989) 49
- [7] B. Lampe: Fortschr. Phys. 40 (1992) 329

- [8] M. Cacciari, M. Greco: Nucl. Phys. B 421 (1994) 530
- [9] B.A. Kniehl, M. Krämer, G. Kramer, M. Spira: Phys. Lett. B 356 (1995) 539
- [10] M. Cacciari, M. Greco: Z. Phys. C 69 (1996) 459
- [11] B. Mele, P. Nason: Nucl. Phys. B 361 (1991) 626; P. Nason, C. Oleari: Report Nos. CERN-TH/97-209, IFUM 588/FT, hep-ph/9709358 (September 1997)
- [12] C. Peterson, D. Schlatter, I. Schmitt, P.M. Zerwas: Phys. Rev. D 27 (1983) 105
- [13] For a compilation of e^+e^- data, see G.D. Lafferty, P.I. Reeves, M.R. Whalley: J. Phys. G 21 (1995) A1
- [14] G. Altarelli, G. Parisi: Nucl. Phys. B 126 (1977) 298
- [15] M. Cacciari, M. Greco, B.A. Kniehl, M. Krämer, G. Kramer, M. Spira: Nucl. Phys. B 466 (1996) 173
- [16] D. Buskulic et al. (ALEPH Collaboration): Z. Phys. C 62 (1994) 1
- [17] R. Akers et al. (OPAL Collaboration): Z. Phys. C 67 (1995) 27
- [18] H. Albrecht et al. (ARGUS Collaboration): Z. Phys. C 52 (1991) 353; D. Bortoletto et al. (CLEO Collaboration): Phys. Rev. D 45 (1992) 21
- [19] J. Chrin: Z. Phys. C 36 (1987) 163
- [20] S. Frixione, P. Nason, G. Ridolfi: Nucl. Phys. B 454 (1995) 3
- [21] M. Cacciari, M. Greco, S. Rolli, A. Tanzini: Phys. Rev. D 55 (1997) 2736
- [22] F.M. Borzumati, B.A. Kniehl, G. Kramer: Z. Phys. C 59 (1993) 341; B.A. Kniehl, G. Kramer: Z. Phys. C 62 (1994) 53
- [23] P. Aurenche, R. Baier, A. Douiri, M. Fontannaz, D. Schiff: Nucl. Phys. B 286 (1987) 553
- [24] F. Aversa, P. Chiappetta, M. Greco, J.Ph. Guillet: Nucl. Phys. B 327 (1989) 105
- [25] H.L. Lai, J. Huston, S. Kuhlmann, F. Olness, J. Owens, D. Soper, W.K. Tung, H. Weerts: Phys. Rev. D 55 (1997) 1280; W.K. Tung (private communication)
- [26] M. Glück, E. Reya, A. Vogt: Phys. Rev. D 46 (1992) 1973
- [27] A.D. Martin, W.J. Stirling, R.G. Roberts: Phys. Lett. B 354 (1995) 155
- [28] L.E. Gordon, J.K. Storrow: Nucl. Phys. B 489 (1997) 405; L.E. Gordon (private communication)

- [29] M. Drees, R.M. Godbole: in Proceedings of Photon '95 Incorporating the Xth International Workshop on Gamma-Gamma Collisions and Related Processes, Sheffield, U.K., 8–13 April 1995, edited by D.J. Miller, S.L. Cartwright, V. Khoze (World Scientific, Singapore, 1995) p. 123
- [30] J. Binnewies, B.A. Kniehl, G. Kramer: Report Nos. DESY 97–012, MPI/PhT/97–009, hep-ph/9702406 (February 1997), Z. Phys. C (in press)
- [31] M. Cacciari, M. Greco: Phys. Rev. D 55 (1997) 7134

FIGURE CAPTIONS

Figure 1: NLO p_T distribution $d\sigma/dp_T$, integrated over $-1.5 < y_{lab} < 1$, of inclusive $D^{*\pm}$ photoproduction in ep scattering with untagged positrons as in the ZEUS experiment. The branching ratio $B(c \rightarrow D^{*+})$ is taken to be unity. The fragmentation models A–F are described in the text.

Figure 2: NLO y_{lab} distribution $d^2\sigma/dy_{lab} dp_T$, at $p_T = 7$ GeV, of inclusive $D^{*\pm}$ photoproduction in ep scattering with untagged positrons as in the ZEUS experiment. The branching ratio $B(c \rightarrow D^{*+})$ is taken to be unity. The fragmentation models A–F are described in the text.

Figure 3: NLO y_{lab} distribution $d^2\sigma/dy_{lab} dp_T$, at $p_T = 7$ GeV, of inclusive $D^{*\pm}$ photoproduction in ep scattering with untagged positrons as in the ZEUS experiment. The NLO-evolved Peterson FF is used in connection with the massive-charm factorization scheme (case E). The branching ratio $B(c \rightarrow D^{*+})$ is taken to be unity. The contributions due to direct (dashed line) and resolved (dash-dotted line) photoproduction are shown together with their sum (solid line).

Figure 4: Influence of the proton PDF's. The total result of Fig. 3 with the CTEQ4M set (solid line) is compared with the corresponding calculations with the charm density inside the proton switched off (dashed line) and with the MRS(G) set (dash-dotted line).

Figure 5: Influence of the photon PDF's. The total result of Fig. 3 with the GRV set (solid line) is compared with the corresponding calculations with the charm density inside the photon switched off (dashed line) and with the GS set (dash-dotted line). For comparison, also the direct-photon contribution of Fig. 3 is shown (dotted line).

Figure 6: Dependence on ξ , where $\mu = M_f/2 = \xi m_T$. The total result of Fig. 3 with $\xi = 1$ (solid line) is compared with the corresponding calculations with $\xi = 1/2$ (dashed line) and 2 (dash-dotted line) as well as the one with $\mu = M_f = m_T$ (dotted line).

Figure 7: Dependence on the parameters ϵ and μ_0 of the Peterson FF. The total result of Fig. 3 with $\epsilon = 0.06$ and $\mu_0 = 2m$ (solid line) is compared with the corresponding calculations with $\epsilon = 0.04$ (dashed line), $\epsilon = 0.08$ (dash-dotted line) and $\mu_0 = m$ (dotted line).

Figure 8: The p_T distributions $d\sigma/dp_T$, integrated over $-1.5 < y_{lab} < 1$, of inclusive $D^{*\pm}$ photoproduction in ep scattering with (a) tagged and (b) untagged positrons as measured by H1 and with (c) untagged positrons as measured by ZEUS are compared with the corresponding NLO predictions with $\xi = 1$ (solid lines), $\xi = 1/2$ (dashed lines) and $\xi = 2$ (dash-dotted lines).

Figure 9: The y_{lab} distributions $d\sigma/dy_{lab}$, integrated over p_T , of inclusive $D^{*\pm}$ photoproduction in ep scattering with (a) tagged and (b) untagged positrons as measured by H1 ($2.5 \text{ GeV} < p_T < 10 \text{ GeV}$) and with (c) untagged positrons as measured by ZEUS ($3 \text{ GeV} < p_T < 12 \text{ GeV}$) are compared with the corresponding NLO predictions with $\xi = 1$ (solid lines), $\xi = 1/2$ (dashed lines) and $\xi = 2$ (dash-dotted lines).

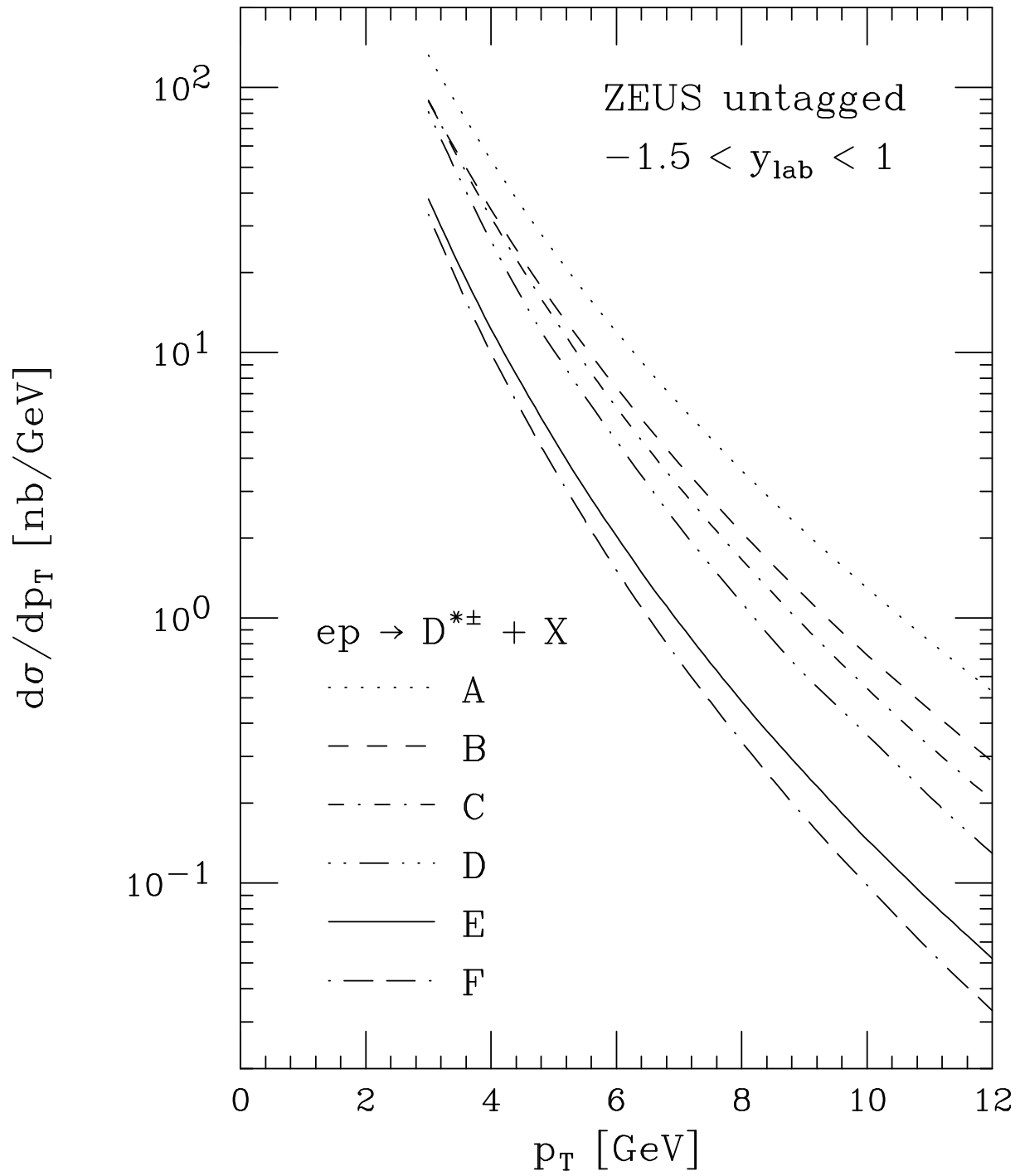


Fig. 1

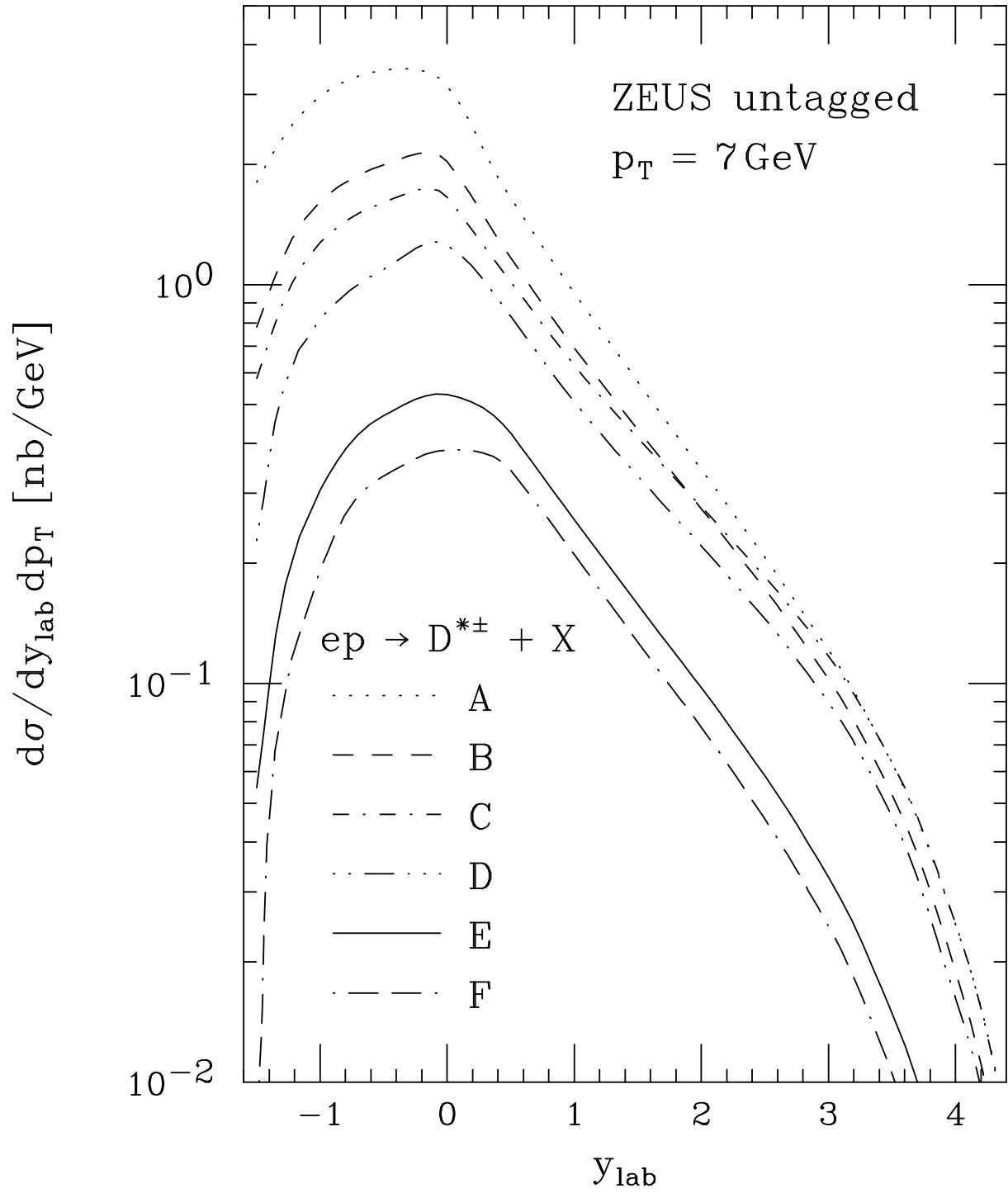


Fig. 2

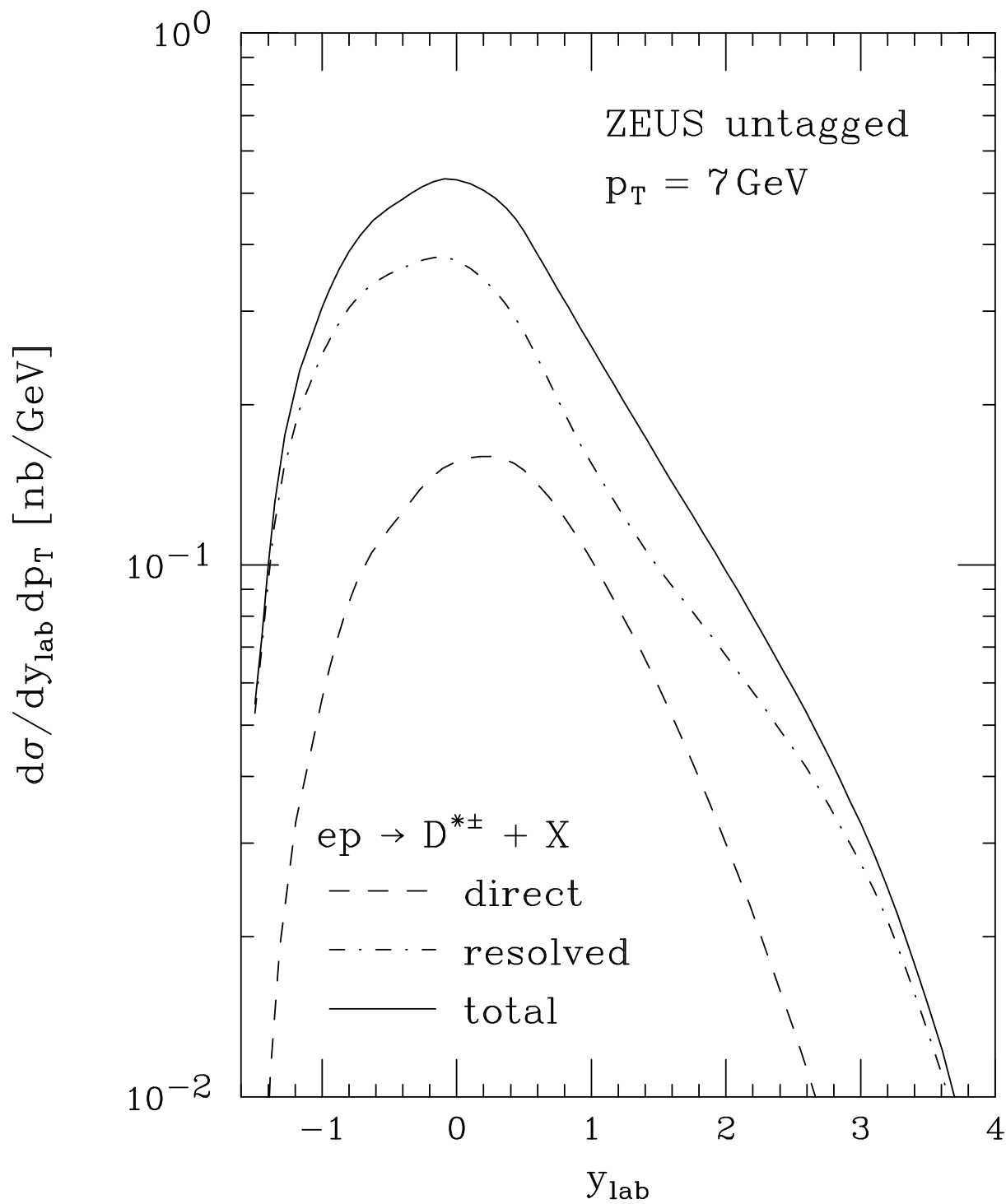


Fig. 3

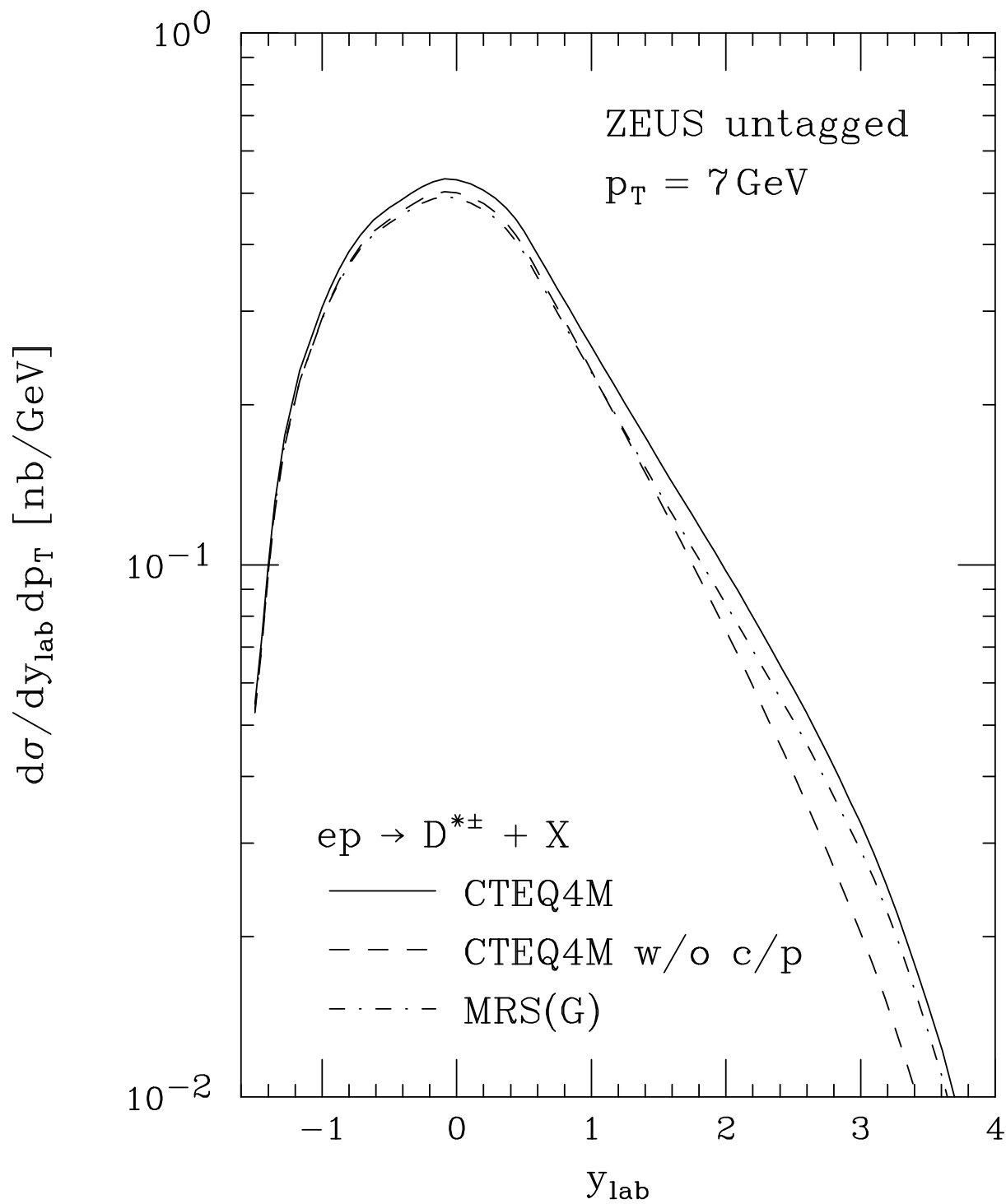


Fig. 4

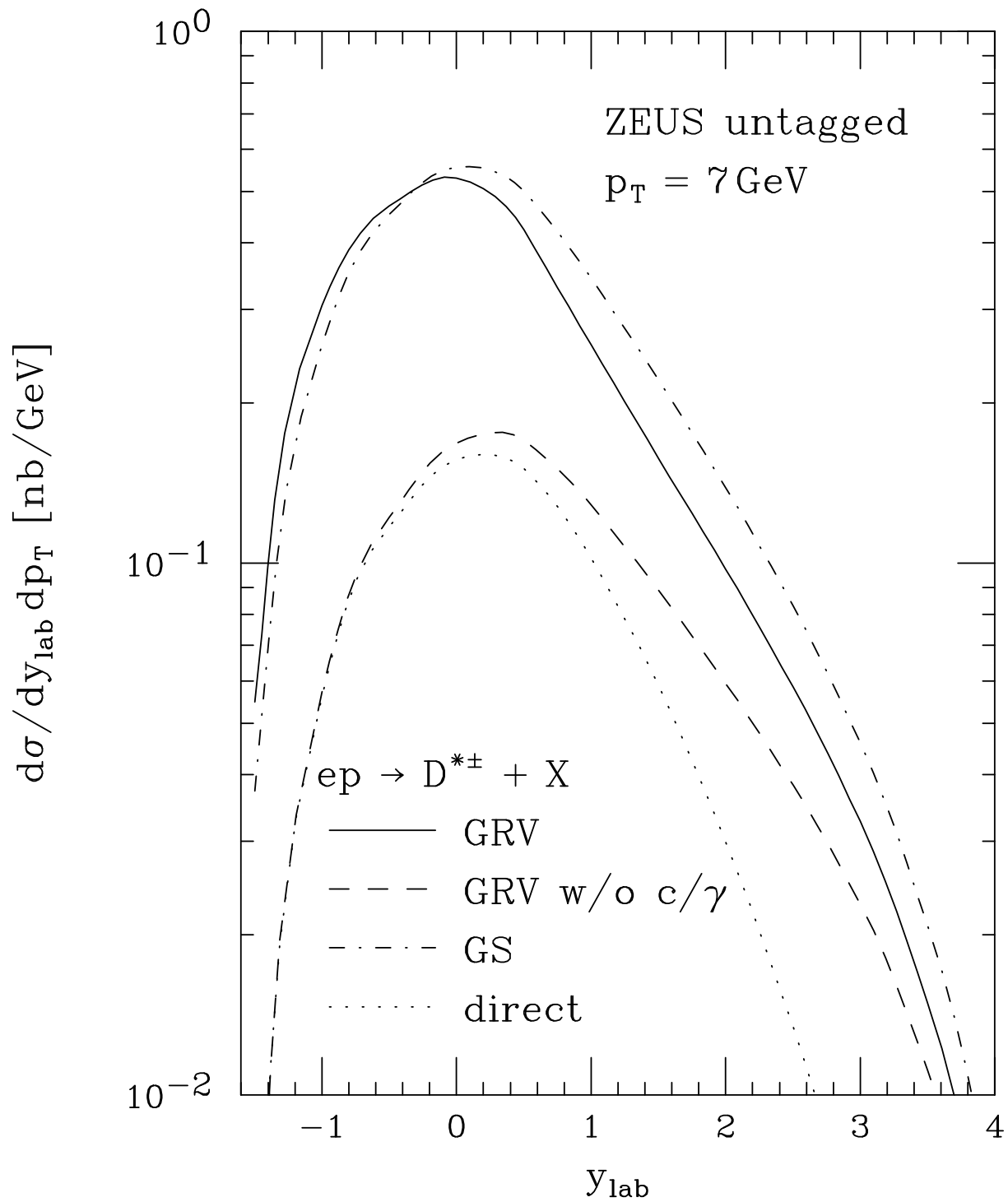


Fig. 5

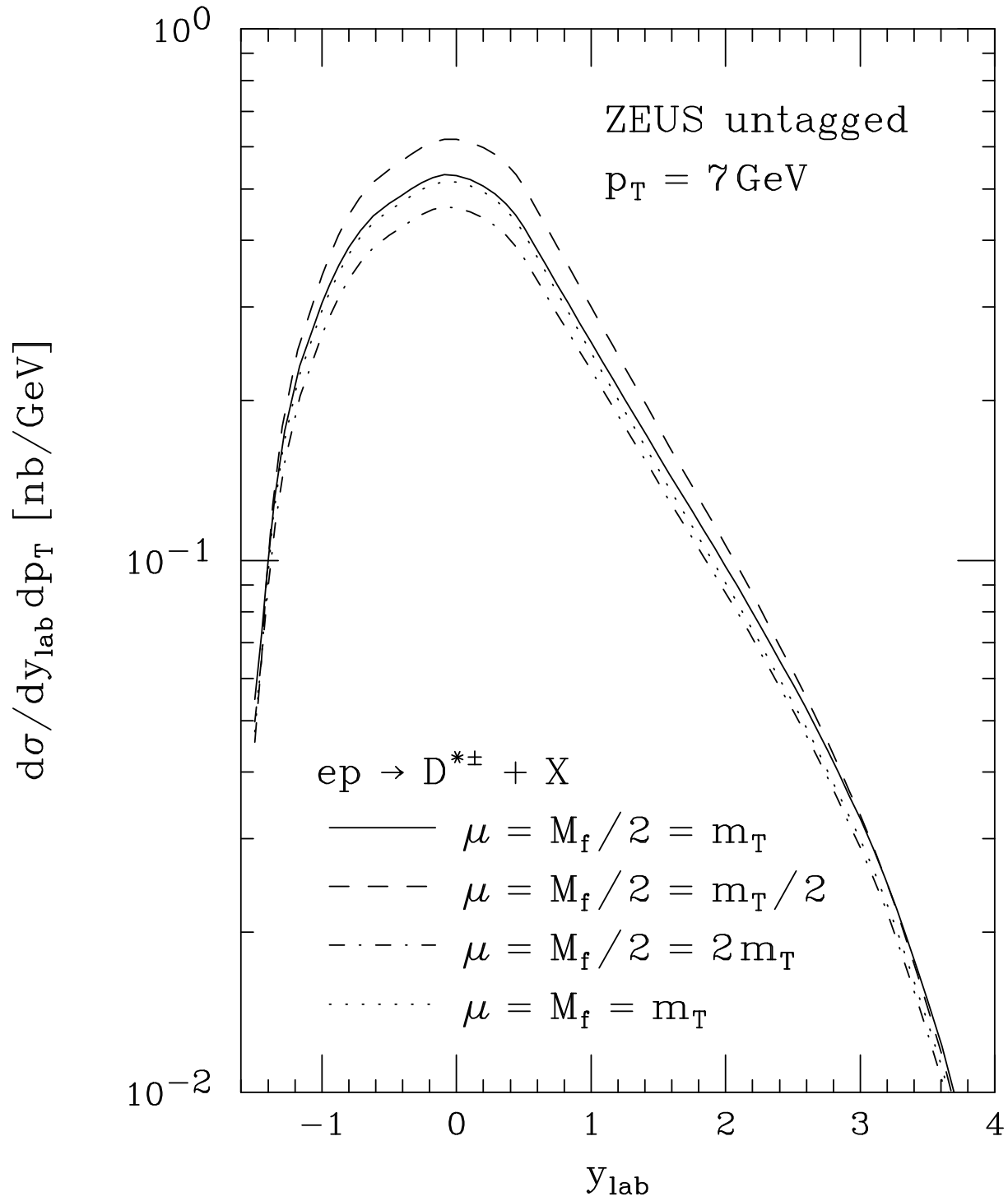


Fig. 6

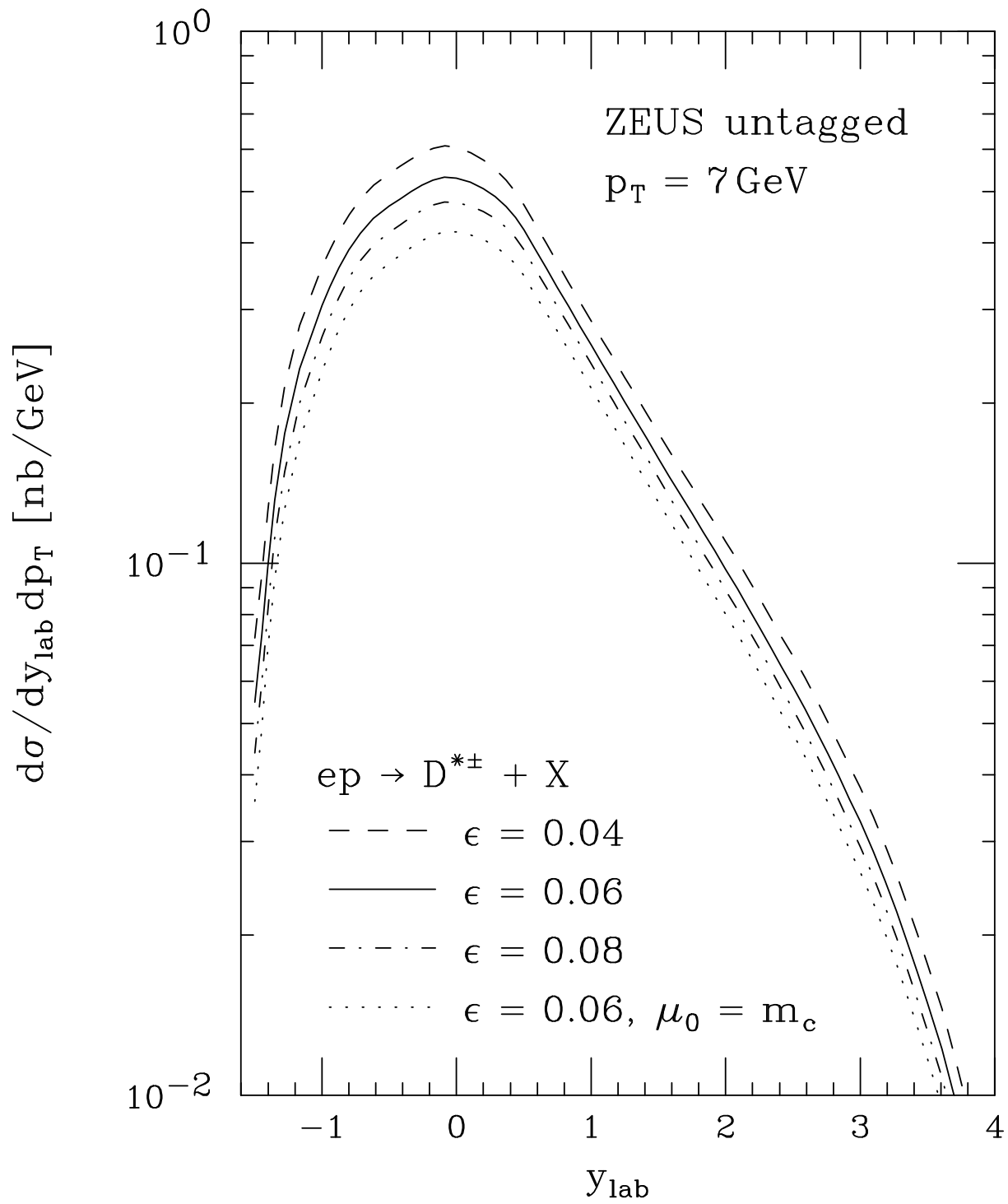


Fig. 7

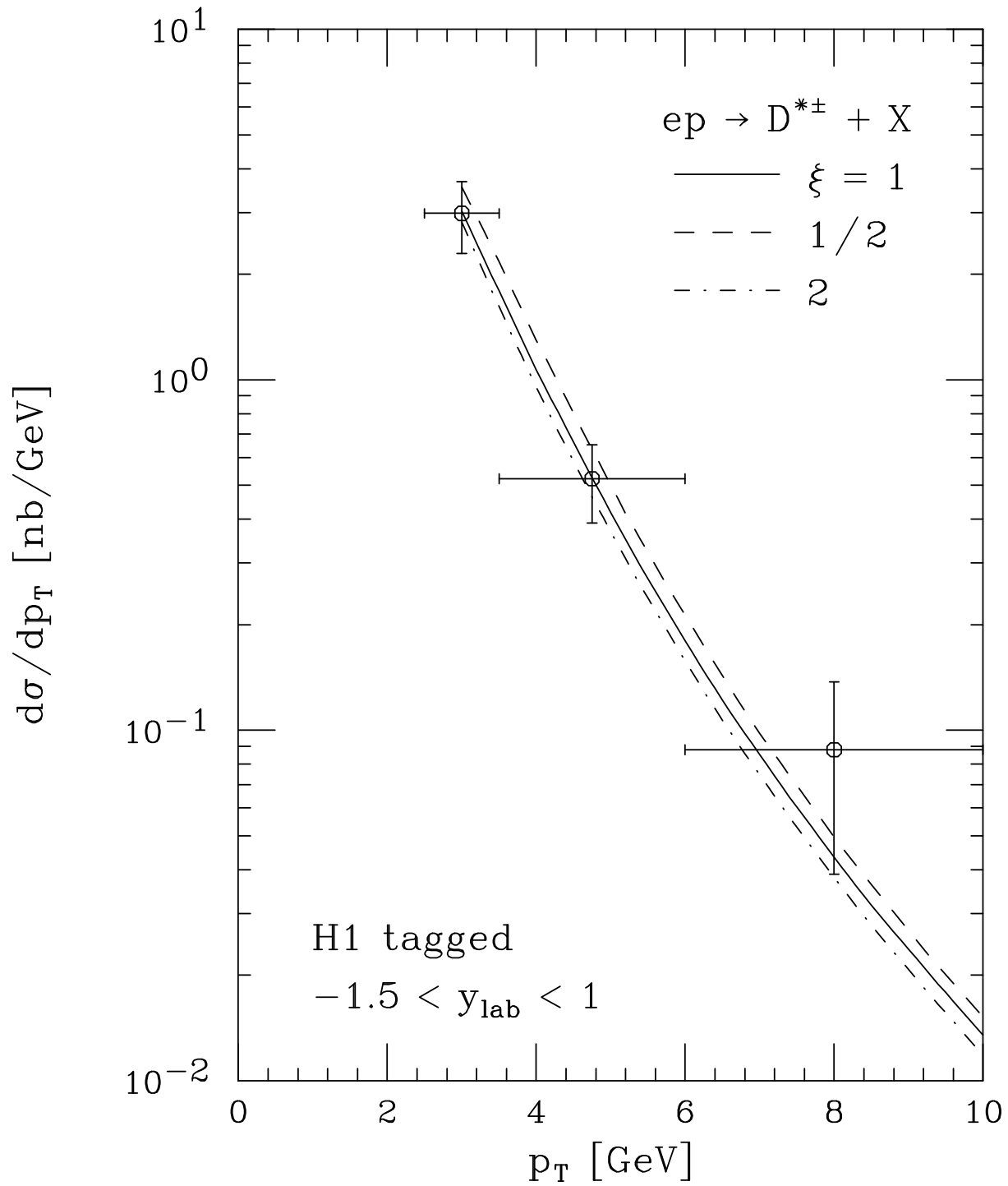


Fig. 8a

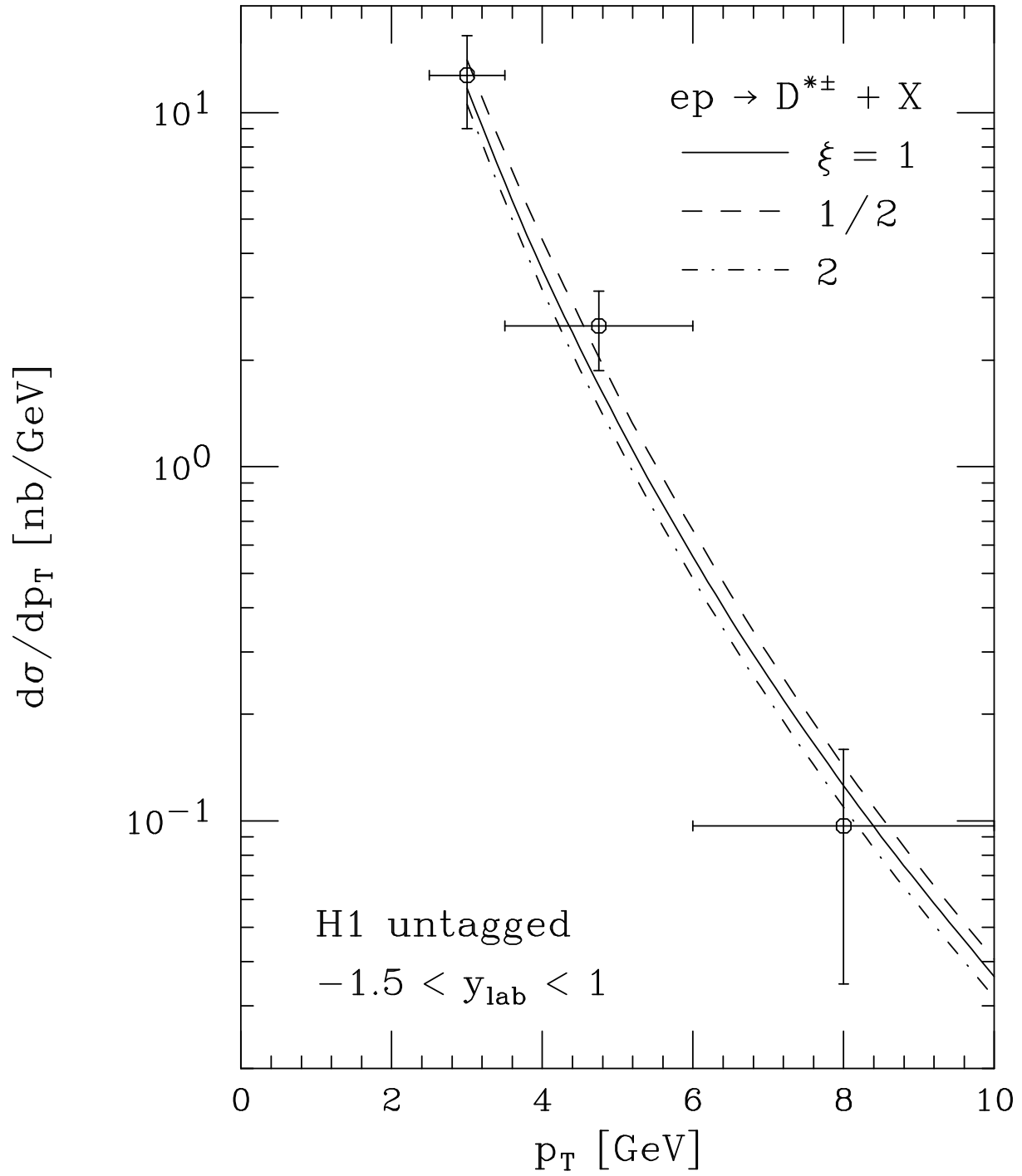


Fig. 8b

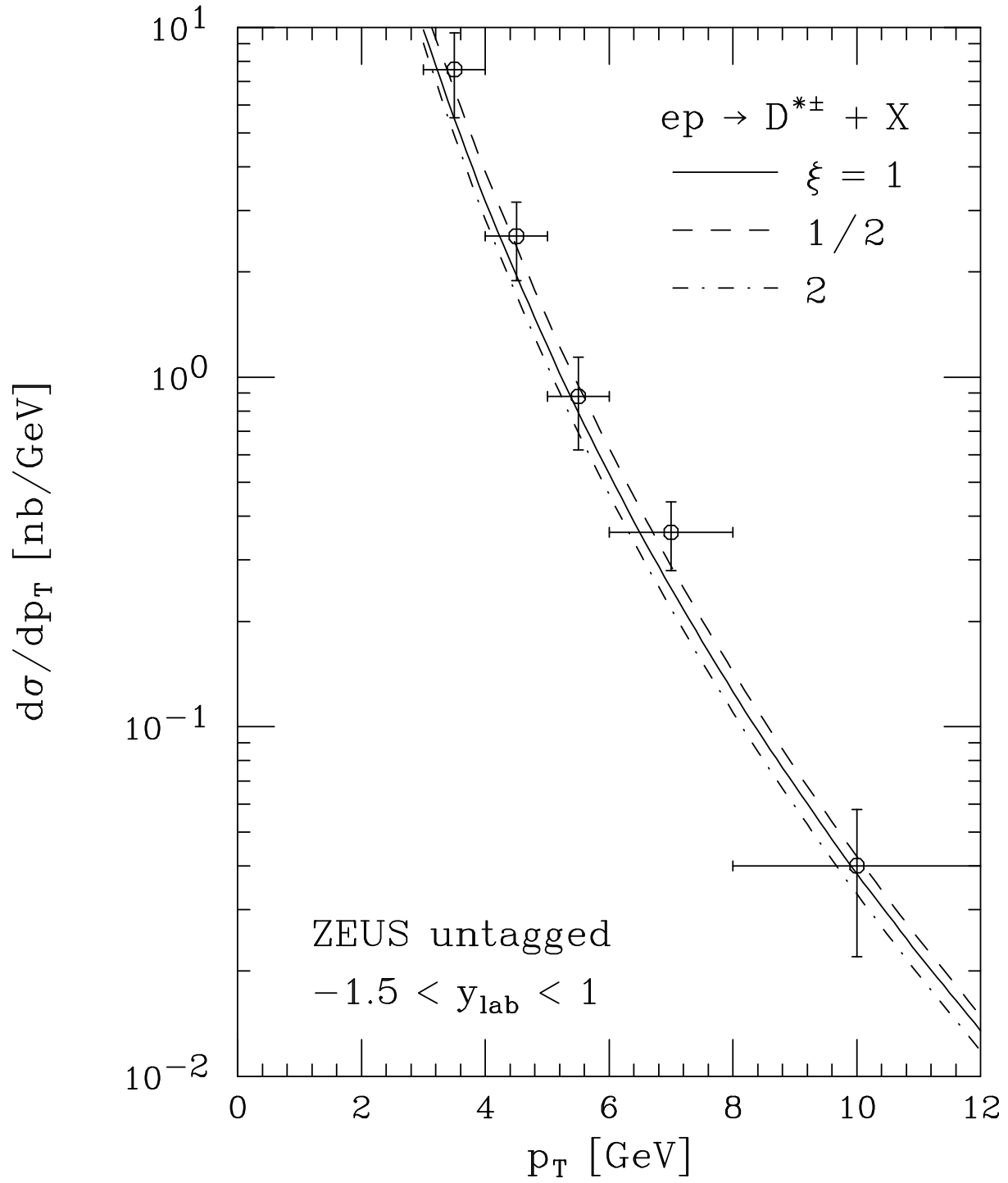


Fig. 8c

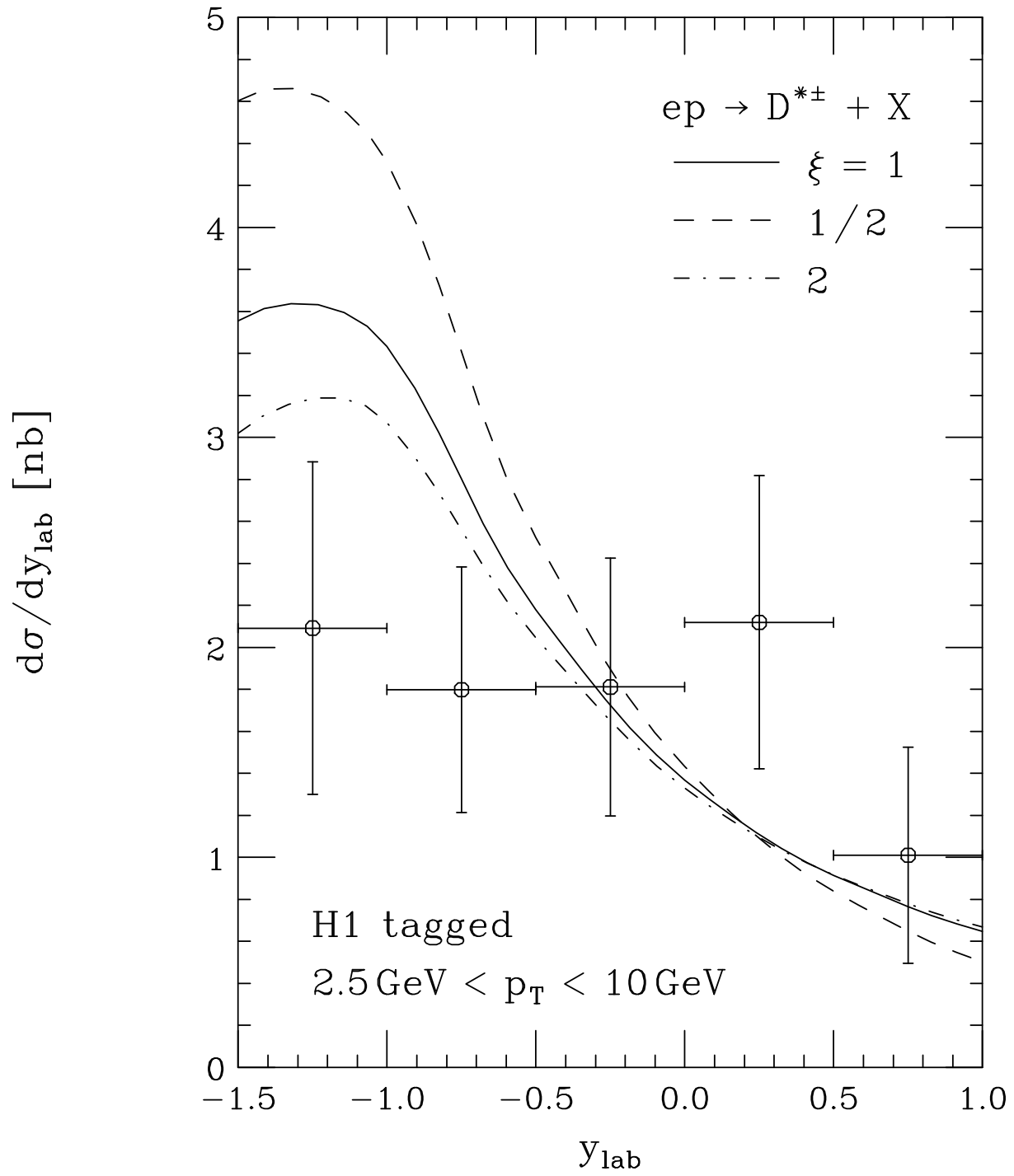


Fig. 9a

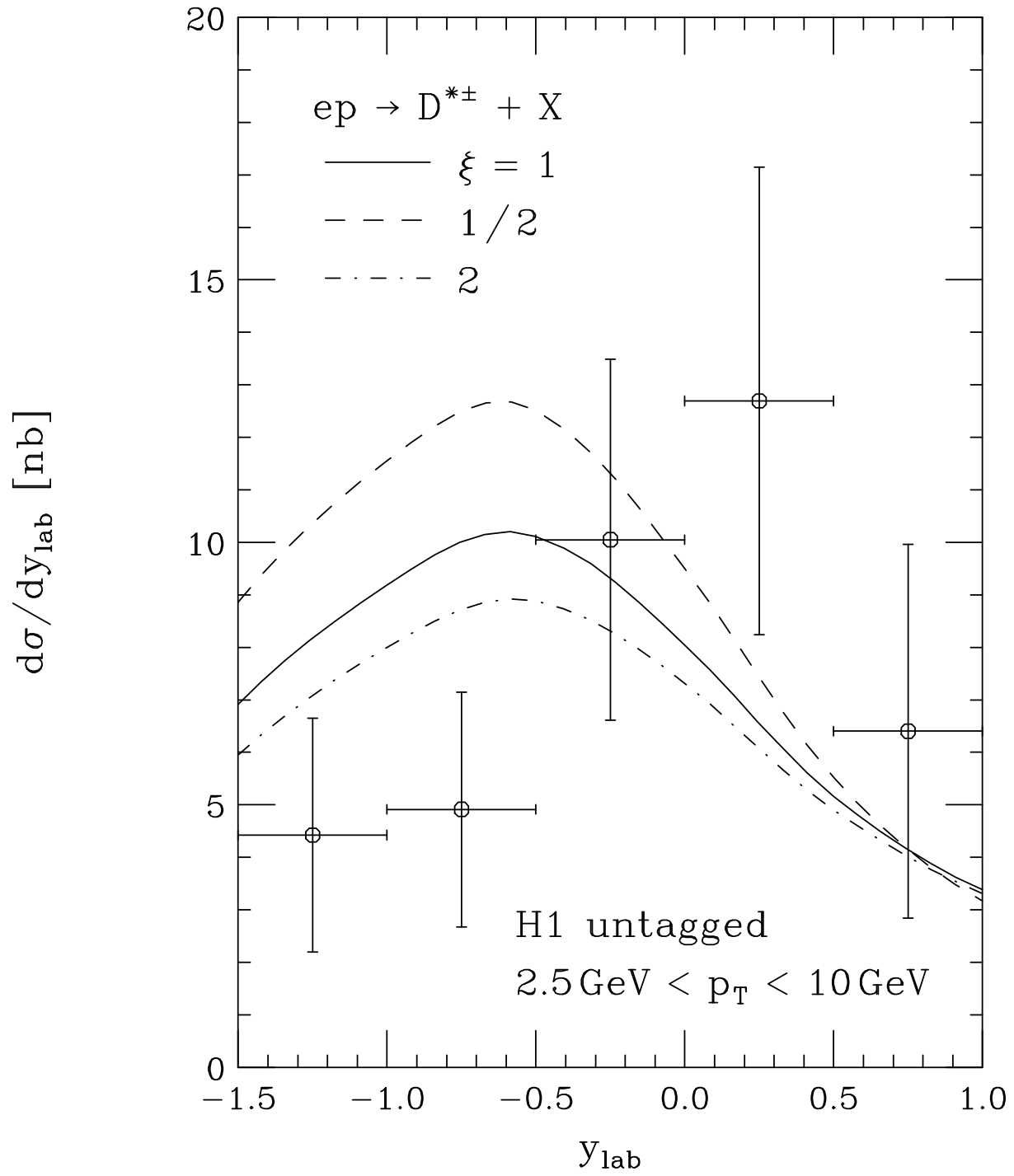


Fig. 9b

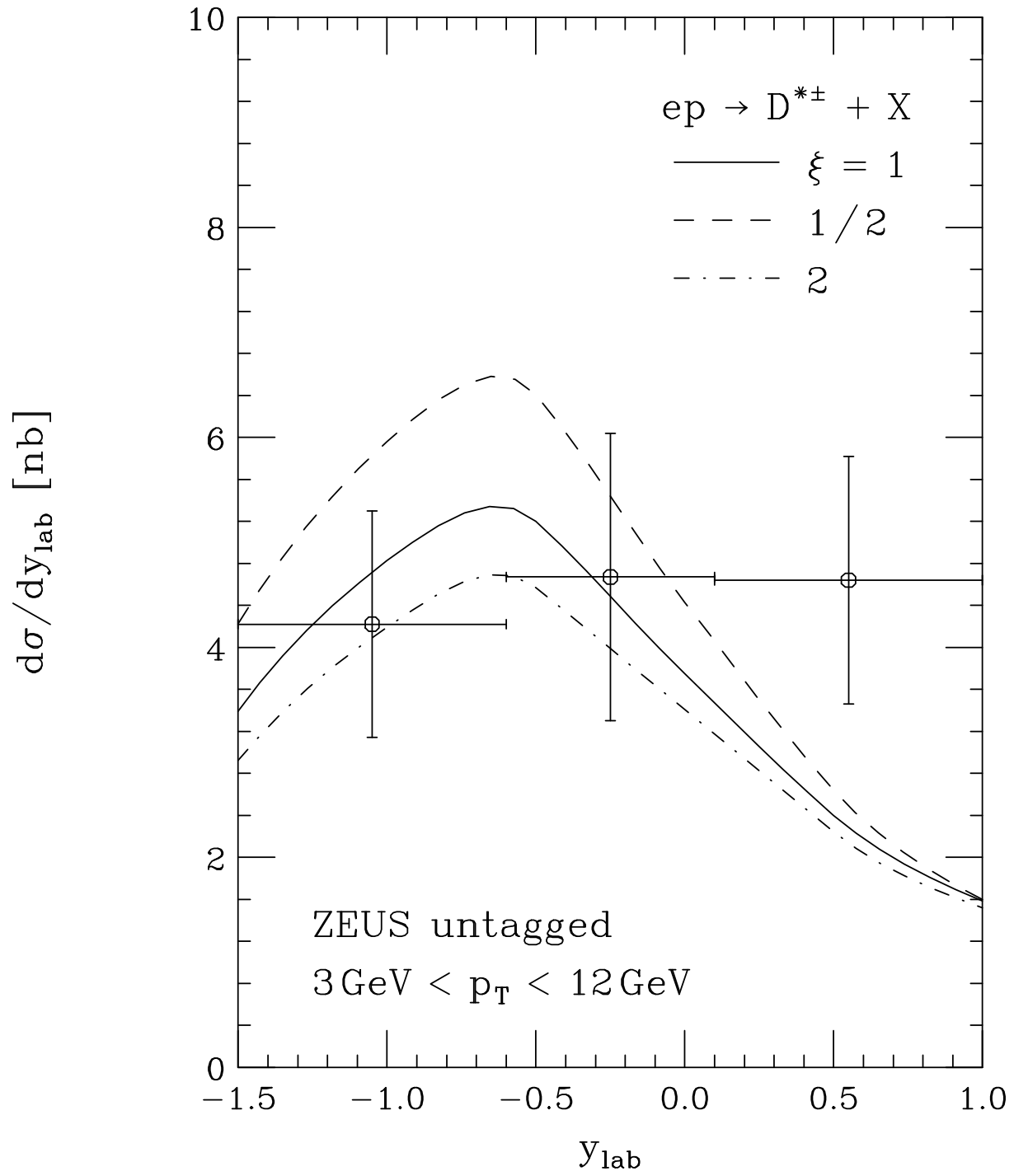


Fig. 9c